Variability in Damage Equivalence Metrics between Heavy Ions and Neutrons

D. B. King, E. Bielejec, P. J. Griffin, K. J. McDonald, G. Vizkelethy, P. J. Cooper, and R. M. Fleming

Sandia National Laboratories: PO Box 5800, Albuquerque, NM, 87185-1146, dbking@sandia,gov

There is an ongoing effort to use heavy ion damage to simulate displacement damage from neutrons. The concept of "equivalent" damage between two types of irradiation is a topic of much interest. This paper examines the variation/consistency between several measured damage metrics from neutrons and ions from particle accelerators. Metrics considered include measured early- and late-time gain degradation in transistors, the type and number of defects as measured in deep level transient spectroscopy (DLTS), and calculated metrics such as the ratio of freely migrating defects to cluster defect or the size of a defect cluster. Careful selection of ion energies and fluences can achieve good agreement with the time dependent degradation occurring from neutron irradiations.

I. INTRODUCTION

The issue of ion-to-neutron damage correlation is of current interest because of the lack of fast neutron sources in the United States. Example applications for fast neutrons studies include displacement-induced embrittlement in reactor pressure vessel materials, efficiency degradation in solar cells, gain degradation in bipolar transistors, and many more. As of October 1, 2006, Sandia National Laboratories (SNL) shut down the Sandia Pulsed Reactor (SPR-III). The Qualification Alternatives to the Sandia Pulsed Reactor (QASPR) Program was initiated at SNL to ensure continuity in electronics qualification after the shut down of SPR-III. The goal of QASPR is to develop a system to qualify the transient response of future electronic systems for short-pulsed fast-neutron environments without relying on testing at a fast-burst reactor. The methodology being developed consists of high-fidelity computational models, initially validated by SPR-III tests, combined with testing of actual devices of interest at alternative experimental facilities such as the SNL Ion-Beam Laboratory (IBL), the SNL Annular Core Research Reactor (ACRR), the SNL Gamma Irradiation Facility (GIF), and the spallation-neutron source at the Blue Room of the Los Alamos Neutron Science Center (LANSCE). While no single facility can replace SPR-III's unique capabilities (high neutron flux, short pulse width, and large uniform test volume) this combination of test facilities and the QASPR methodology will allow a complete representation of the expected physics parameters needed to correlate neutron and ion damage. The use of multiple facilities requires the program modelers and experimentalists to understand how damage in one facility relates to damage in the other alternate facilities. The selection of damage metrics is key to understanding these damage relationships. The successful implementation of the modeling/testing system would allow Sandia to predict electronic response, with uncertainty quantification, to a wide variety of radiation conditions.

In this paper, we compare selected damage metrics for devices irradiated at the IBL using high energy heavy ions and devices tested in SPR-III with a neutron fast fission spectrum. The key element here is to identify the amount of facility-to-facility variation in the different damage metrics. The metrics identified include experimental quantities such as the measurement of late-time and early-time performance of transistors exposed to the various radiation sources as well as calculated metrics such as displacement kerma. Late-time experimental metrics are generally gathered on the transistor after the pulse or after an elevated temperature bake-out procedure has been performed on irradiated transistors. Early-time metrics are gathered during the entire radiation pulse as well as during the anneal stages after the radiation pulse. Late-time metrics include the Messenger-Spratt damage factor (defined by equation (2)), deep level transient spectroscopy (DLTS), capacitance-voltage (CV) sweeps, and Gummel (or recombination current) measurements. Early-time metrics include transient gain, Annealing Factor (defined by equation (4)), DLTS spectra at cryogenic temperatures (≥20K), and active gain measurements at cryogenic temperature.

II. EXPERIMENTAL DETAILS

Single diffusion lot 2n2222 npn bipolar junction transistors from Microsemi were used in these

experiments to minimize and control the device to device variation present in commercial off-the-shelf (COTS) parts. Construction analysis, secondary ion mass spectroscopy (SIMS), and spreading resistance profile (SRP) measurements were performed on these devices to accurately determine the device geometry and doping profile of the active region of the devices. These parameters are extremely important for understanding and modeling the defect formation and transport during both ion and neutron irradiations. 2n2222 devices were chosen for these experiments because they are a well-established technology, and silicon has a considerable history of documented defect literature and extensive data base.

The ion irradiations were performed at the IBL. The heavy ion beams were produced by a 6 MV tandem Van de Graaff accelerator. The current ranges from a few pAs to a few hundred nAs depending on the energy of the beam and the ion species. The ion beam was focused to a size somewhat larger than the size of the transistor die (~0.5x0.5 mm^2) and was pulsed for single irradiations ranging from 10 μs to 10 ms using electrostatic deflection plates and a high voltage switch with rise and fall times of 150 ns. The currents of the transistor were monitored using current viewing resistors before, during, and after the shots. The voltages across the current viewing resistors were recorded with a Yokogawa DL750P oscilloscope-recorder. The circuit diagram for the ion irradiation experiment is shown in Figure 1 with red lettering indicating the measurement points. The transistors were operated in constant emitter current mode, provided by a current limiting diode biased to -15 V on the emitter leg. The base-collector junction was reverse-biased with 10 V on the collector. The base leg was tied to ground through a relatively large resistor to ensure an accurate measurement of the base current prior to the shot. The additional clipping diode located on the base leg was used to prevent large base potential excursions despite the large photocurrent response to the ion beam.

The neutron irradiations were performed at the SPR-III central cavity over a wide range of neutron fluences. SPR-III is a fast burst reactor, which can be operated in either a steady-state or pulsed mode. A maximum total neutron fluence of $5x10^{14}$ n/cm^2 ($3.9x10^{14}$ n/cm^2 1 MeV Si equivalent), maximum dose of 120 krad(Si), and a FWHM of 100 μs is possible in single pulsed mode. The devices were placed in the SPR-III central cavity to achieve maximum neutron fluence and because the neutron spectrum is a relatively unmoderated, well characterized, fission spectrum. The operation of the transistors was monitored prior to, during, and for 100 seconds after each shot. For SPR-III operations, the circuit described above was modified by removing the clipping diode from the base leg.

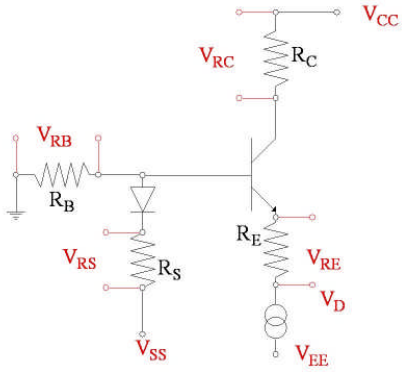

Fig. 1. The experimental circuit used in the ion irradiations. SPR irradiations did not include the clipping diode in the base leg.

Displacement damage results when an incident particle (either a neutron or ion) creates silicon recoils that move from their original lattice sites. This silicon recoil atom then undergoes further collisions with other lattice atoms creating a collision cascade. This results in the formation of Frenkel pairs (vacancy interstitial pairs) in the silicon bipolar junction transistors, which shorten carrier lifetime and degrade the gain. One of the key differences between ion and neutron irradiations is the method by which they transfer energy to the silicon lattice. Neutrons have a very small collision cross-section with Si atoms (no Coulomb interaction); therefore, most neutrons pass through the device without striking a Si atom. Those neutrons that do strike a Si atom cause localized collision cascades; therefore neutron damage is created uniformly throughout the device. Ions lose energy continuously as they travel through the device by Coulomb scattering (interaction with the target nuclei) and ionization (interaction with electrons). The net result is that, for incident ions, Frenkel pair creation varies as a function of penetration depth with a majority of the displacement damage created at the end-of-range of the ion trajectory. The effect of the end-of-range damage is further complicated by the geometry of the device. In Figure 2(a) we show a cross-sectional view of the Microsemi 2n2222 device. The two main regions of interest are the active areas of the device directly under the emitter contact and the field oxide region over the emitter diffusion (between the emitter and base contact fingers). The relative areas of each of these key regions are indicated on the figure. In Figures 2(b) and 2(c) we plot the penetration depth for 4.5 and 36 MeV Si ions as determined from SRIM[4] for each of the two regions. These energies are chosen as a representative low and high energy example. In the case of the 4.5 MeV Si irradiation, the end-of-range is in the Al metallization for the emitter contact region; whereas for the field oxide region, the end of range is at the base-emitter junction and produces a damage peak in the junction. The 36 MeV Si irradiation damage peaks occur

in the device substrate. A discussion of the effect of the ion penetration depth will follow below.

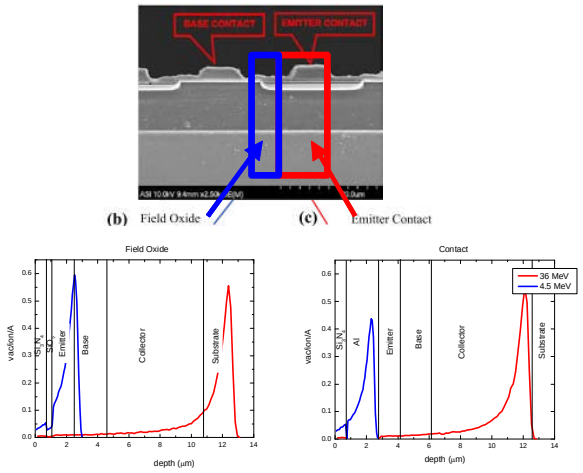

Fig. 2. (a) Cross-sectional view of a Microsemi 2n2222 device stained to show the emitter, base and collector diffusions. The area surrounded by the red box corresponds to the active area of the device (the base-emitter junction) that is below the emitter metallization. The area inside the blue box corresponds to the active area of the device covered by the field oxide between the emitter and base contacts. (b) and (c) show the end of range depth from a SRIM calculation for 4.5 and 36 MeV Si for the two regions described above.

III. ACTIVE GAIN TEST RESULTS

The temporal transistor response to SPR-III and IBL irradiation environments are quite different due to the nature of the radiation and the time profile of the irradiation conditions. We will discuss the following three representative irradiations from SPR-III and the IBL: 1) a SPR-III maximum pulse with a total neutron fluence of 3.9×10^{14} n/cm^2 (1 MeV Si equivalent), a total dose of 1.2×10^5 rad(Si), and a pulse width of 100 μS (FWHM), 2) a 4.5 MeV Si ion irradiation with a pulse width of 75 μs and an ion fluence of 2×10^9 ions/cm^2, and 3) a 36 MeV Si ion irradiation with a pulse width of 100 μs and an ion fluence of 2.7×10^9 ions/cm^2. Figure 3 illustrates the collector and base current behavior (IC and IB, respectively) of a 2n2222 bipolar junction transistor with a nominal constant emitter current bias of 9.0 mA for the SPR-III irradiation. The combined gamma/neutron ionization during the pulse causes an increase in IC (from 9 mA to 11.5 mA) and IB (from 86 μA to -3 mA) due to the photocurrent generated in the transistor junctions by the ionization. The neutron degradation is masked during the pulse by the transient photocurrent. The circuit measuring convention defines the photocurrent response in IC to be positive and in IB to be negative. As the ionization component of the pulse decreases, the neutron damage effect on IC and IB becomes evident. IC decreases from a nominal current of 9 mA to 5.5 mA. IB increases from 86 μA to 7 mA. As the neutron component of the pulse decreases, both IB and IC begin to anneal. IB decreases and IC increases during the anneal phase.

The Si collector and base current responses for the 4.5 MeV and 36 MeV Si irradiations are pictured in Figure 4 and Figure 5, respectively. Very little photocurrent is observed for 4.5 MeV Si irradiation because the ion end-of-range was selected to occur at the base-emitter junction; in fact, a combination of degradation and annealing response is observed through the pulse (to 75 μs). The annealing response is observed to occur in the base and collector currents at the end of the Si pulse. The 36 MeV Si irradiation generates peak photocurrents on the order of 60 to 95 mA (other 36 MeV irradiation conditions with higher beam currents can generate twice as much). The photocurrents are primarily generated in the transistor junctions. Figure 6 shows a close up of the post-irradiation base and collector current annealing responses. The IBL allows the measurement of early time response because the ionization environment stops immediately with the pulse.

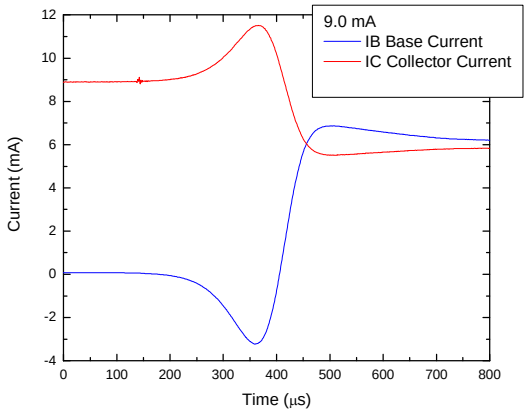

Fig. 3. Base and collector current response to a maximum pulse at the SPR-III facility. The nominal emitter current is 9 mA.

IV. DISCUSSION OF DAMAGE METRICS

The displacement damage, or non-ionizing energy loss (NIEL), is one traditional metric for correlating damage from different irradiation environments. The displacement kerma can be defined for ion irradiations, but it can not be assumed to represent an "equivalent" neutron damage response in a semiconductor, or other material, until the correlation between measured device

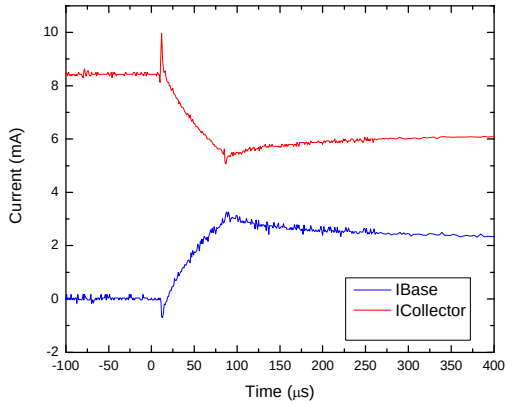

Fig. 4. Base and collector current response to a 4.5 MeV Si ion pulse at the IBL facility. The nominal emitter current is 9 mA.

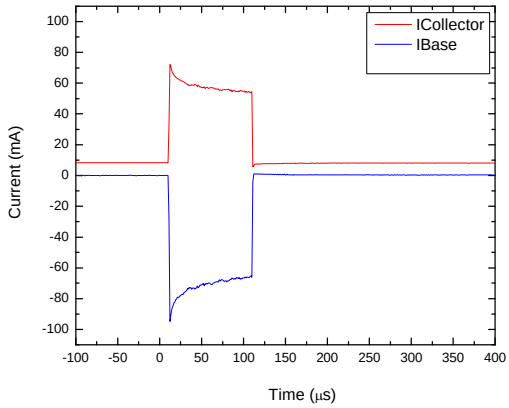

Fig. 5. Base and collector current response to a 36 MeV Si ion pulse at the IBL facility. The nominal emitter current is 9 mA.

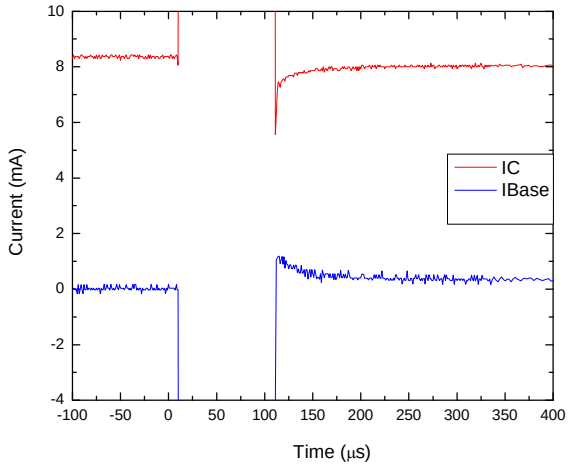

Fig. 6. Close-up depiction of the base and collector current response to a 36 MeV Si ion pulse at the IBL facility. The nominal emitter current is 9 mA.

degradation metric (e.g. carrier lifetime, gain, etc.) and the calculated metric (NIEL or displacement kerma) is validated. A study of the variability of experimental and calculated damage metrics for a 2n2222A npn transistor has been carried out. The following sections discuss a range of experimental and calculated metrics and shed light on the potential variability of any desired "equivalence" used to describe the damage.

IV.A. Late-time Transistor Gain Measurements

The late-time gain degradation for each radiation environment affords some insight in comparing IBL environments (fluence and primary ion energy variations) to each other and with the SPR environment. We will begin by comparing the inverse gain degradation Δ(1/G) as defined by Eqn. (1) (Ref. 1),

$$\Delta\left(\frac{1}{G}\right) = \frac{1}{G_\infty} - \frac{1}{G_0}, \qquad (1)$$

where G_∞ is the final late-time gain, and G_0 is the initial gain. For G_∞, we have used a post ASTM[2] anneal gain as the final gain value. This anneal (80 ºC for 2 hours) is designed to aid in comparisons of stable late-time damage created by different irradiation conditions. Past work had found it difficult to compare late-time gains because of the inconsistent conditions for the time selected to measure G_∞ and due to changes in storage temperature and device bias during the intervening time. After the ASTM anneal, further room temperature annealing has not been observed[2]. Plotting the inverse gain degradation as a function of radiation fluence, we calculate the device damage factors (k) for each radiation field using the Messenger-Spratt equation[1] :

$$\Delta\left(\frac{1}{G}\right) = k \cdot \Phi, \qquad (2)$$

where Φ is the total facility fluence. For a reactor environment, Φ is typically expressed as a neutron spectrum damage constant times the 1 MeV (Si) equivalent neutron fluence.

Figure 7 shows the inverse gain degradation dependence on the ion fluence for the 4.5 and 36 MeV Si beams with two emitter currents (0.22 mA and 9 mA). All four Si curves follow the Messenger-Spratt equation and the damage factors are calculated by a linear fit to the data sets. The 4.5 MeV Si has the largest slope (largest

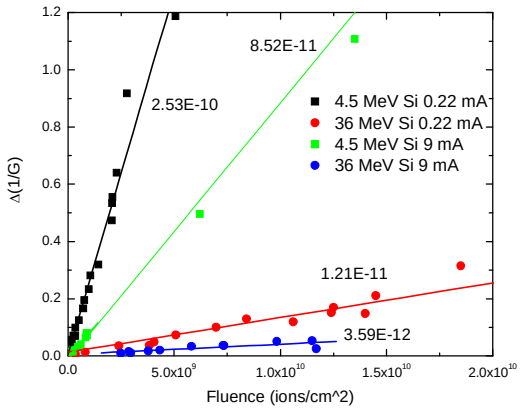

Fig. 7. The inverse gain degradation for 4.5 and 36 MeV energy Si ions as a function of fluence for an emitter currents of 0.22 and 9 mA. The device damage factor, k, is included with each energy level and bias.

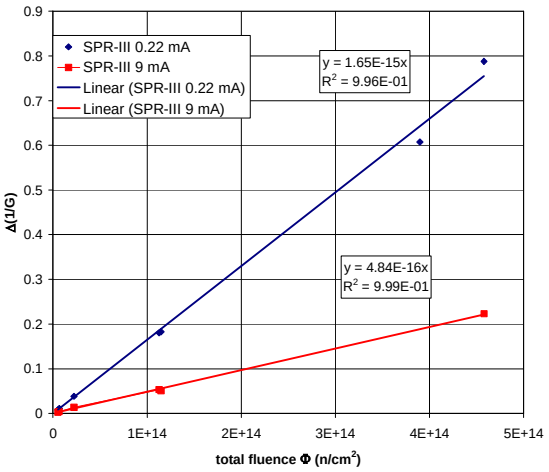

Fig. 8. The inverse gain degradation is shown for a SPR-III irradiation as a function of fluence for emitter currents of 0.22 and 9 mA.

damage factor) due to the ion end-of-range at the emitter-base junction. Work by the QASPR team has indicated that the gain degradation of the silicon bipolar junction transistors (BJTs) is dominated by recombination at the base-emitter junction for low emitter current. Also, larger emitter currents result in smaller damage factors and enhanced annealing during the irradiation due to increased electron density. Figure 8 shows the inverse gain degradation dependence on the neutron fluence for the same two emitter currents above; the higher emitter current has the lowest damage factor. One goal of the QASPR work is to compare a Messenger-Spratt formulation of the ion damage factor, defined to be the gain degradation for various heavy ions, to the damage factor measured for neutrons of a given spectrum. This allows us to define one type of damage "equivalency" metric and to relate an "effective" ion fluence to neutron fluence, through gain degradation, as in Eqn (3).

$$\Phi_{neutron} = \frac{k_{ion}}{k_{neutron}} \Phi_{ion} \,. \qquad (3)$$

IV.B. Calculated Frenkel Pair Damage Metrics

Reference 3 has previously reported that SRIM[4] calculations have found that ratios of the gain degradation in the 2N2222A with different ions and energies, as well as for neutrons, closely track ratios in the calculated displacement kerma. MARLOWE[5] calculations are reported here. These calculations look at a wider set of damage-related metrics. MARLOWE has been used to produce detailed maps of the Frenkel pair locations. Damage clusters are then defined by collections of defects that are within one lattice constant of each other. Isolated defects are defined to be defects that are not associated with a cluster. The defects within the cluster region are defined as cluster defects. Note that both interstitials and vacancies are counted as defects, and that the number of interstitials and vacancies within the cluster do not have to match due to the energy imparted to the interstitials on a collision and their subsequent movement. Similarly vacancies can be filled or moved in the MARLOWE transport process.

Table 1: Variability of Damage Metrics Calculated with MARLOWE

Si Ion Energy	MARLOWE Calculated Metric			
	C_{size}	C_{ratio}	C_{vol}	Ax_{ratio}
1.00 keV	4.301	0.6351	4.727	1.2087
5.00 keV	3.625	0.6136	3.843	1.3185
10.0 keV	3.659	0.6126	3.812	1.3008
50.0 keV	3.647	0.6017	3.762	1.2966
100. keV	3.667	0.6024	3.923	1.2859
500. keV	3.611	0.5958	3.808	1.2955
1.00 MeV	3.579	0.5941	3.821	1.2931
5.00 MeV	3.555	0.5916	3.740	1.2921
10.0 MeV	3.544	0.5919	3.720	1.2915
50.0 MeV	3.237	0.5877	3.425	1.2916
% max. var. (all eng.)	32.8%	8.1%	38.%	9.1%
% max. var. (E >= 5 keV)	13.3%	4.4%	14.5%	2.5%
Calculated with identical electronic and nuclear potentials, displacement threshold energy, cascade generation parameters.				

It must also be noted that MARLOWE is a binary collision approximation (BCA) code, accurate down to energies of about 100 eV, but not a molecular dynamics code that can follow actual defect formation. Thus, this modeling does not permit one to simulate associated interstitials and vacancies with more complex configurations, such as a divacancy or a vacancy-phosphorus defect. MARLOWE is a Monte Carlo simulation. The results reported here were run with enough statistical samples that the number of Frenkel pairs had a statistical uncertainty of between 1% and 3%. Table 1 shows the variation in some defect/cluster metrics for incident silicon ions at a range of energies. The Table 1 metrics, reported in each column, correspond to:

- C_{size} = number of defects per cluster
- C_{ratio} = ratio of defects located in a cluster to total defects
- C_{vol} = volume of a cluster when fitted with an ellipsoidal shape
- Ax_{ratio} = ratio of the major-to-minor axis of the ellipse fit to capture the cluster volume

Row 11 of the table shows that the variation in the cluster size and volume could be over 30% as the ion energy varies, but that the ratio of clustered and isolated defects, as well as the cluster geometry, were fairly constant (to within 10%). However, when one only looks at the data for incident ion energies above 5 keV, the data in column 12 show that the variation in the cluster size/volume collapsed to only ~10%, and the ratio of isolated-to-cluster defects and in the cluster shape were negligible. This behavior is consistent with an interpretation that cascades for all ion energies have similar behavior for these damage metrics once the ion energy is sufficient to begin to spawn new branches/clusters. As the ion energy increase, we just get more or the same type of damage structures.

Note that the metrics above were computed over the total damage cascade. The Frenkel pair creation process is dominant in the end-of-ion-range region. When externally applied ions, as opposed to neutron-induced recoils, are used to establish a "neutron-to-ion" damage correlation in the behavior of a semiconductor, it is only the part of the ion track in the sensitive device volume that matters. Figure 2 showed some of the sensitivity of the damage to the device geometric details for a Microsemi 2N2222A. In light of the above ion energy sensitivity and in order to examine the effect of damage by different parts of the cascade, we repeated the above analysis using only a thin silicon slab in order to investigate the energy-dependent behavior of the early part of an ion track. In this case we saw a dramatic variation in the calculated metrics. The following observations could be made:

- The vacancy per ion rate dropped by a factor of 5 for a 1 keV ions and by a factor of 8.5 for a 1 MeV ions
- The number of clusters per ion varied by a factor of 9 for 1 keV ions and 14.7 for a 1 MeV ions
- C_{size} varied by a factor of 4.7 for 1 keV ions and by 1.2 for 1 MeV ions.
- The cluster shape was fairly consistent in all cases

One conclusion that can be drawn from this range of calculated metrics is that, above a certain energy, the in total cascade damage looks to have little variation, but that parts of the cascade structure can vary dramatically with respect to postulated damage metrics. Thus, great care must be taken in the interpretation and correlation of calculated or experimental damage metrics gathered on testing objects that have a small sensitive volume.

IV.C. Experimental Time-Dependent Metrics

Figure 9 illustrates the transient gain for the SPR-III and 4.5 MeV silicon irradiations. Vertical lines indicate photocurrent interference for the SPR-III irradiation. The transistor gain response is of critical interest as many engineering/circuit requirements and functionality will be dependent on the gain behavior prior to, during and immediately after the irradiation. This gain is difficult to use as a direct facility-to-facility comparison because it is dependent on the temporal response of the radiation, emitter current, temperature, initial gain of the device, and gain of the device at the end of the irradiation pulse. Another time metric that incorporates the gain response with initial gain and final gain and eases the comparison of transistor performance from facility-to-facility is the annealing factor.

In Figure 10 we show a comparison between the annealing factor for a 4.5 MeV Si exposure and a SPR-III shot with the late-time $\Delta(1/G)$ on the order of unity for both exposures. The $\Delta(1/G)$ value was the primary factor in choosing the IBL fluence level to use in comparing with the SPR shot. The annealing factor[6] is defined as the following,

$$\text{Annealing Factor} = \frac{1/G(t) - 1/G_{initial}}{1/G_{\infty} - 1/G_{initial}} \qquad (4)$$

The annealing factor is the ratio of inverse gain measurements on the device, but is selected because it relates the number of radiation-induced defects at time, t, compared to the number of permanent (late-time) radiation-induced defects.

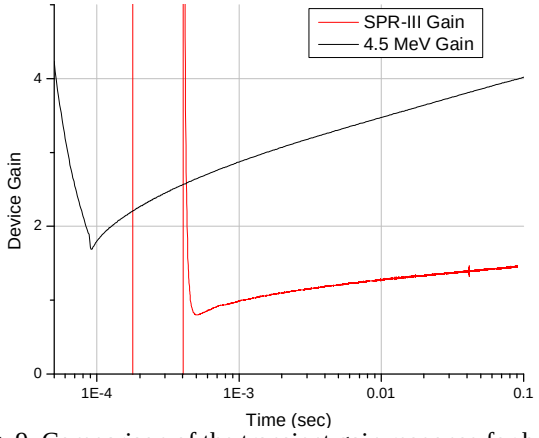

Fig. 9. Comparison of the transient gain response for both ion and fast neutron irradiation. Both devices have a nominal emitter current of 9 mA.

This formulation, subtracting the inverse initial gain and dividing by the late-time change in inverse gain, is used to normalize out both the initial gain and the fluence variation between irradiations. In both the SPR-III and IBL cases we have a pulse length on the order of 100 μs with final gain on the order of unity. The early-time comparison ($<10^{-3}$ s) with SPR-III is of limited value because of late-time gamma-induced photocurrent which masks the response of the device in the fast neutron experiments. These early-time gammas are caused by the delayed fission product decay. The oscillations observed in the data are a real phenomena due to physical oscillations (ringing) of the reactor fuel after the shot induced by the fuel heating. This ringing actually corresponds to an increase in the fissions (prompt fission neutrons and gammas) as the fuel assembly compresses in each fuel oscillation. The subsequent comparison indicates good agreement between the time dependence of the ion and neutron irradiations. At this point in time we have made no attempt to match the time base between the two facilities. The neutron pulse is characterized by a full-width-at-half-maximum (FWHM) of 100 μs, but the radiation pulse has an extended fission tail. The IBL pulse is a sharp well-defined square pulse. The peak of the neutron-induced gain degradation is significantly later (~300 μs) in time as compared to the peak of the IBL pulse. As we are comparing the two facilities from early to late times this small effect of shifting the time axis does not affect the overall conclusions that we can draw from this figure. Given the caveats mentioned above, we are working to demonstrate that we can correlate the 1-MeV (Si) neutron equivalent fluence to the ion fluence with respect to the gain degradation metric.

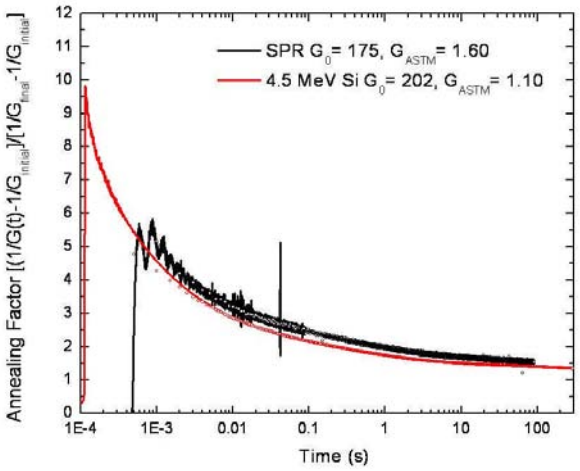

Fig. 10. Comparison of the early-time transient response for both ion and fast neutron irradiation. The annealing factor shows a similar response for both ions and neutrons.

IV.D. Cryogenic Defect Behavior

While monitoring active gain degradation has been an important transient metric for assessing transistor damage, we can also measure gain at low temperatures in the region of carrier freeze-out and then heat the transistors to watch the defect evolution, as measured by gain, with temperature. In this test, the actively biased transistor is cooled to 30K and irradiated. While measuring gain, the transistor is then heated to room temperature (referred to as Cycle 1), cooled back down to 30K, and then re-heated to room temperature (Cycle 2). Figures 11 and 12 show the results of this test sequence for two transistor biases. This test was performed at SPR-III and the IBL. An equivalent fluence of $3x10^{13}$ n/cm^2 was targeted at each radiation facility. Δ(1/G) and equation 3 were used to select an ion fluence that would result in comparable damage and 1 MeV neutron equivalent fluence between a neutron and ion facility. The measured gain was normalized to the value measured at room temperature. This test examines the combined effects of time, temperature, and current-injection annealing. For cycle 1, we observe that the 1 mA bias transistor has greater normalized gain recovery compared to the 1 μA bias transistor due to enhanced current injection annealing. For cycle 2, the normalized gain recovery for the 1 mA bias is not significantly greater than the 1 μA bias transistor. Two heating cycles are used to assess the importance of transistor bias and injection annealing versus thermal heating. The two cycles are widely separated for transistors with low bias current; the separation indicates that thermal heating plays a major role in annealing defects. Transistors with high bias have closely spaced thermal cycles. This indicates

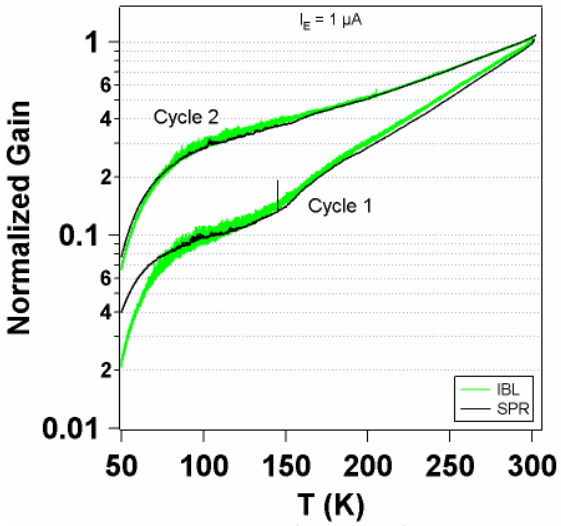

Fig. 11. Gain response as a function of transistor temperature and bias at 1 μA.

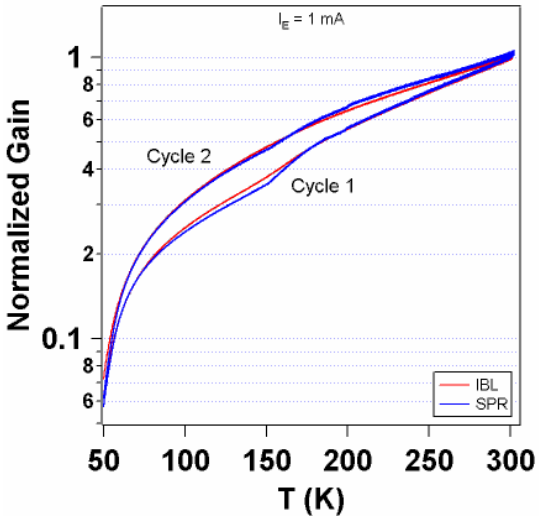

Fig. 12. Gain response as a function of transistor temperature and bias at 1 mA.

that current injection due to the increased bias is an important component in annealing defects and that both temperature and bias have a combined effect and must be treated in tandem. The annealing shape and agreement of normalized gain between SPR-III and IBL is good; the agreement indicates that similar annealing kinetics occur after the initial defect formation for both irradiation environments.

IV.E. Microscopic Defect Metrics

The neutron-induced gain degradation is related to the introduction of specific types of lattice defects. Deep level transient spectroscopy (DLTS) techniques[7] can be used to measure defect populations (or at least relative populations between different types of irradiation fields). A DLTS spectrum consists of measurements of the characteristic changes in the capacitance of a pn junction as a function of temperature. The capacitance changes result from the filling and emptying of the defect complexes. Neutron, electron, and heavy ion irradiation can result in different relative ratios of defect types[8]. Figure 13 illustrates this for DLTS signals that have been measured in the collector region and normalized to the divacancy peak. An electron radiation from the White Sands Missile Range Linear Accelerator (WSMR LINAC), SPR-III, and the IBL (at 28 MeV and 48 MeV) are included. At 95 K and 135 K, the vacancy-oxygen (VO) and shallow divacancy (V_2) defects are measured. At 233 K, a complex of defects are measured that include the deep divacancy and higher order defects (most likely vacancy related). This large peak is the hallmark of neutron or ion-damaged silicon, both of which have damage clusters. Electron damage produces more uniform displacement damage. The higher order defects are absent, leaving nearly equal V_2 peaks.

While the general structure of the DLTS plots are the same for the different irradiation types, one of the key differences is that the number of deep level defects formed in the neutron irradiation is much larger than that formed in either the ion or electron irradiations. While we do not yet have a definitive explanation of this effect we identify two possible causes: ionization and micro-structure. We first note that the neutron irradiation has the largest deep level defect and also has the lowest ionization. The electron irradiation (largest ionization) shows the least deep level defects. The ionization associated with the ion irradiation, although large, decreases dramatically at the end-of-range of the ion track. The 28 MeV Si, which has an end-of-range in the collector of the device, would have an effectively smaller ionization as compared to the 48 MeV Si which has an end-of-range in the device substrate. A second potential explanation involves the microstructure of the clusters due to the irradiation. For electrons we expect uniform damage with widely spaced defects similar to ion tracks away from their end-of-range. Conversely, ions near the end-of-range and neutrons are expected to be similar with large amounts of clustering. This implies that 28 MeV Si with its end-of-range in the collector should be more neutron-like and the 48 MeV Si with its end-of-range in the substrate should be more electron-like. Indeed, this is observed in the DLTS plots. Clustering calculations indicate that 4.5 MeV Si is the most neutron-like, but has no observable signal in the discussed base-collector DLTS[9].

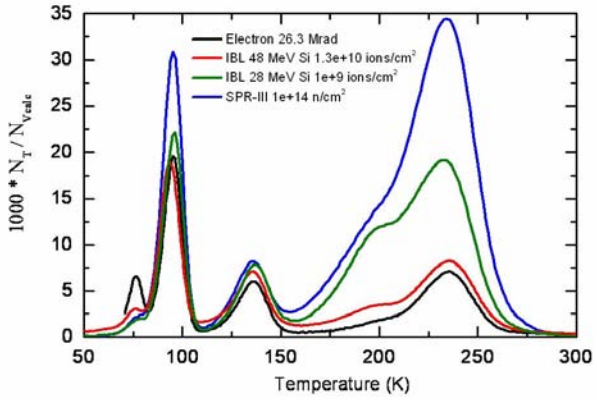

Fig. 13. Selected DLTS spectra for irradiation at IBL, SPR, and the WSMR LINAC are shown. High ion energy approximates electron damage. Low ion energy approximates SPR damage.

Future work is planned to further exploit the information in a DLTS signature in the pnp device. DLTS work can measure defect formation in the base of a pnp bipolar junction transistor. The pnp base is more heavily doped than the collector of the npn, and other defect types (such as the vacancy phosphorous) will be characterized as a function of radiation type and fluence and their effects on gain will be measured. This will allow for a direct comparison between low energy Si irradiations that directly target the base-emitter junction, such as 4.5 MeV Si, and neutron irradiations. Transistors can be annealed after radiation damage, and DLTS peaks will be compared to gain annealing as a function of temperature. The integral of the deep level DLTS signals can be compared to the recombination current in a damaged transistor as a function of fluence.

V. CONCLUSIONS

We have presented the variation in several metrics used to compare ion and fast neutron irradiations. These metrics can be used to assess the damage relations or correlations for bipolar transistor response. Ultimately, we seek to state a correlation between device damage observed in both neutron and ion radiation environments. This correlation can be the basis for the definition of a damage-mode specific "equivalence". A combination of metrics will be needed to ensure a comprehensive understanding of the physics involved in the ion-to-neutron damage correlation.

ACKNOWLEDGMENTS

We acknowledge the outstanding support of D. L. Buller in running and maintaining the IBL, the SPR-III reactor staff, and the members of the QASPR experimental team. Sandia is a multiprogram laboratory operated by Sandia Corporation, a Lockheed-Martin Company, for the United States Department of Energy's National Nuclear Security Administration under contract DE-AC04-94AL85000.

REFERENCES

1. G. C. Messenger and M. S. Ash, "The Effect of Radiation on Electronics Systems," New York: Van Nostrand Reinhold, 1986.
2. ASTM Standard Number E1855-05e1 (ASTM International, West Conshoken, PA, 2005) www.astm.org
3. E. Bielejec *et al*., "Damage Equivalence of Heavy Ions in Silicon Bipolar Junction Transistors", *IEEE Trans. Nucl. Sci.*, vol. 53, pp 3681-3686, Dec. 2006.
4. www.srim.org
5. Robinson, M.T. and I.M. Torrens, *Computer-Simulaion of Atomic-Displacement Cascades in Solids in Binary-Collision Approximation.* Physical Review B, 1974. **9**(12): p. 5008-5024.
6. T. P. Wrobel and D. C. Evans, IEEE TNS NS-29 (6), 1721 (1982)
7. D. V. Lang, J. Appl. Phys. **45**, 3023 (1974).
8. R. M. Fleming, C. H. Seager, D. V. Lang, E. Bielejec, and J. M. Campbell, Appl. Phys. Lett. **90**, 172105 (2007).
9. S. M. Myers and W. R. Wampler, private communications